COMMON REFLECTION SURFACE-BASED PRESTACK DIFFRACTION SEPARATION

P. Bakhtiari Rad, B. Schwarz, C. Vanelle, and D. Gajewski

email: *parsa.bakhtiari@studium.uni-hamburg.de*

keywords: *diffractions, prestack data enhancement, time migration velocity analysis*

ABSTRACT

Partial CRS stacking is a robust technique in seismic data processing for prestack data enhancement and trace interpolation. In this work, we modify the original partial CRS stack in order to separate diffracted energy from reflections before stacking. Performing the separation prior to stacking permits not only the generation of diffraction-only gathers, but it also leads to better recognition of diffractions and facilitates the building of velocity models for migration operators. We propose a new workflow entirely based on partial CRS to stack every sample of a diffraction event within an aperture expanded in offset and midpoint directions. We show that for the synthetic Sigsbee 2A data set as well as for field data this new workflow can be used to effectively separate reflected and diffracted energy in the prestack domain. It also demonstrates potential for time migration velocity analysis using diffraction-only data.

INTRODUCTION

The importance of diffractions in seismic processing and imaging has recently gained more and more recognition (see, e.g., Dell, 2012). Diffractions carry valuable information about the subsurface in regions with small scale structures, e.g., fractures, pinch-outs, thin lenses, etc. Diffraction imaging can, therefore, lead to higher resolution, which is of particular interest for reservoir characterisation and exploitation. If diffraction-only data are available, they permit to extract information in addition to that obtained from reflection processing. Accordingly, several methods have been suggested to separate diffractions and reflections already in the time domain. A comprehensive overview of such methods is given by Dell et al. (2012).

In this work, we introduce a workflow for prestack diffraction separation based on the 2D common reflection surface (CRS) approach (see, e.g., Müller, 1999; Mann, 2002) and the common diffraction surface stack (e.g., Soleimani et al., 2010). We suggest to combine the technique for diffraction separation by Dell et al. (2012), who suggested a workflow for diffraction imaging that is based on the common reflection surface (CRS) method, with the partial CRS stacking method. The latter was introduced by Baykulov and Gajewski (2009) to achieve prestack data enhancement. It does, however, not distinguish between diffractions and reflections. Dell and Gajewski (2011) applied the separation in the poststack domain. With the new approach, the separation is performed in the prestack domain and leads to enhanced prestack diffraction-only gathers.

One particular advantage of our workflow is that stacking velocities determined from diffraction-only data are actually time migration velocities: whereas velocities obtained by stacking of reflection data depend on the reflector dip, diffractors have no orientation, and thus the velocities obtained from diffraction-only data immediately serve as velocities for time migration (see, e.g., Fomel et al., 2006; Dell et al., 2012).

After a brief outline of the method, we investigate its performance on the synthetic Sigsbee 2A data set as well as on field data.

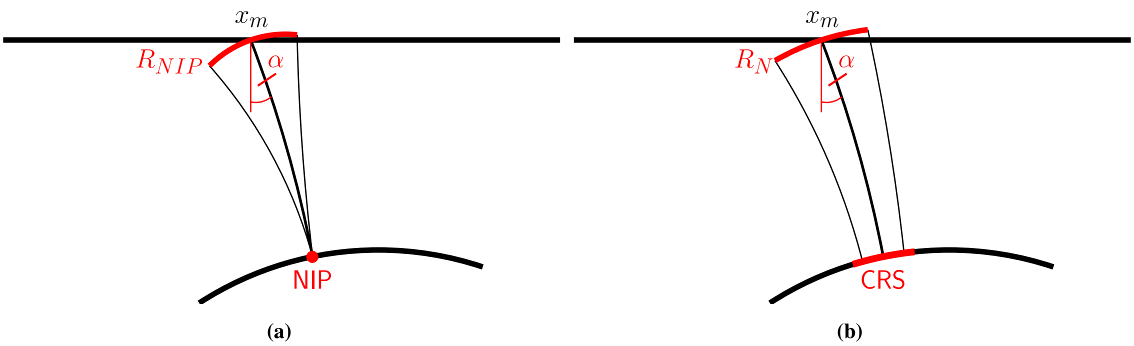

Figure 1: The meaning of the ZO-CRS parameters: (a) R_{NIP} is the radius of curvature of a wavefront emitted by a fictitious point source at the normal incidence point (NIP); (b) R_N is the radius of wavefront curvature of the fictitious so-called normal wave emitted by an exploding reflector element, the common reflection surface (CRS). The incidence angle is denoted by α.

METHOD

Common reflection surface stacking

The CRS stacking operator for the zero-offset (ZO) situation is given by (see, e.g., Schleicher et al., 1993; Müller, 1999):

$$t_{CRS}^2(\Delta x_m, h) = \left(t_0 + \frac{2\sin\alpha}{v_0}\Delta x_m\right)^2 + \frac{2t_0\cos^2\alpha}{v_0}\left(\frac{\Delta x_m^2}{R_N} + \frac{h^2}{R_{NIP}}\right) \quad . \tag{1}$$

It describes the reflection traveltime in the vicinity of the CMP location under consideration, x_0, for deviations in midpoint, $\Delta x_m = x_m - x_0$, and half-offset, h, coordinates. In Equation 1, t_0 is the zero-offset traveltime and v_0 is the velocity in the acquisition surface at the CMP. The three wavefield attributes or CRS parameters are the incidence/emergence angle α at the coinciding source and receiver, the radius R_{NIP} of a fictitious wavefront emitted by a point source at the normal-incidence-point (NIP) on the reflector, and the radius R_N of a fictitious wavefront emitted by a an exploding reflector element surrounding the NIP, the common reflection surface (see Figure 1).

Common diffraction surface stacking

Although Equation 1 was initially derived for reflections it can also be applied for diffractions since, according to Mann (2002), a diffractor can be described by a reflector segment with undefined orientation and infinite curvature. The latter property implies that the common reflection surface shrinks into a point and thus for diffractions $R_N = R_{NIP}$. Therefore, in the diffraction case, Equation 1 simplifies to (see, e.g., Dell and Gajewski, 2011)

$$t_{CDS}^2(\Delta x_m, h) = \left(t_0 + \frac{2\sin\alpha}{v_0}\Delta x_m\right)^2 + \frac{2t_0\cos^2\alpha}{v_0 R_{NIP}}\left(\Delta x_m^2 + h^2\right) \tag{2}$$

If Equation 1 is applied as a stacking operator, the stacked section will contain both reflected and diffracted events. If, however, Equation 2 serves as the operator, the stacking will enhance the diffractions and suppress the reflections, ideally resulting in a diffraction-only stacked section.

In order to successfully apply Equation 2, separation of diffraction and reflection events has to be carried out prior to the stacking with the diffraction-only operator 2. This can be achieved by a comparison of the values for R_N and R_{NIP} after determining them with a semblance analysis using the CRS stack 1.

In practice, we find that for diffractions R_N will be close to R_{NIP}, but the values will in general not coincide exactly. This is due to the band-limited nature of the data as well as the fact that the traveltime expressions 1 and 2 are not exact. To nevertheless ensure a reliable detection, we do not compare the values directly but by means of the weight function introduced by Dell and Gajewski (2011),

$$W_F = \exp\left(-\frac{R_N - R_{NIP}}{R_N + R_{NIP}}\right) \quad . \tag{3}$$

The value of the function W_F is approximately equal to one if R_N is close to R_{NIP}, i.e., the event under consideration is most likely a diffraction. Otherwise, W_F is very small.

Although it may seem intuitive to use W_F as a weight function for the stack, its application does not lead to the desired result of a clean separation of diffractions because too much residual energy from reflections remains in the data. Therefore, we suggest the following alternative: if W_F exceeds a predefined threshold, we weight the stack result with one. If W_F is smaller than the threshold, the weight is zero, which corresponds to assigning the value zero as the stack result. By this weighting procedure, we can effectively remove reflected energy. The choice of the threshold determines the amount of residual reflected energy in the aimed-for diffraction-only stack. If the threshold is chosen too low, reflection events are not fully suppressed. A too high choice of the threshold, on the other hand, can suppress diffracted energy as well. In conclusion, the best suitable threshold depends on the complexity of the medium and the data quality. Investigations of the sensitivity of the threshold function have been carried out by Guntern (2013) and Voß (2013).

Partial CRS

Partial CRS is a robust technique introduced by Baykulov and Gajewski (2009) for prestack data enhancement and offset regularisation. As suggested by the name, a partial stack is carried out over a reduced aperture centred on the half-offset position h_A instead of a full stack around h=0. Accordingly, the stacking result is written not to the zero-offset coordinate $P_0 = (x_0, t_0, h = 0)$ but to the position P_A with the coordinates $(x_0, t_h, h \neq 0)$. Figure 2 illustrates the procedure. It allows to generate a new trace at this position with an increased signal-to-noise ratio due to the stacking. If the stacking result is normalised with the number of contributing traces, the amplitude of the new trace is preserved with respect to the according trace prior to the stacking (Baykulov and Gajewski, 2009). The new trace can, therefore, be considered equivalent to a prestack trace. Repeated application for all offsets thus provides enhanced prestack data.

The prestack data enhancement can be performed for reflections and diffractions. To separate diffraction energy before stacking, we need to decide for each event at a location P_A whether it corresponds to a diffraction or a reflection. In order to make that decision, the CRS parameters at P_A are required. The parameters are, however, only known at P_0. The same problem arises in the subsequent step for the calculation of the CDS operator. Since this issue is independent of the nature of the event, i.e., reflection or diffraction, we use the solution suggested by Baykulov and Gajewski (2009),

$$t_0 = -\frac{h_A^2 \cos^2\alpha}{v_0 R_{NIP}} + \sqrt{\left(\frac{h_A^2 \cos^2\alpha}{v_0 R_{NIP}}\right)^2 + t_A^2}. \tag{4}$$

Once the matching location P_0 has been found, evaluation of the CRS parameters by means of W_F determines if the event at P_A is a diffraction. In that case, the traveltime t_0 is substituted in Equation 2 to construct the partial CDS stacking operator for the point P_A. The subsequent stack then leads to an enhanced prestack diffraction-only section.

In conclusion, we suggest to combine the features of the prestack diffraction separation in the workflow presented in the upcoming section.

WORKFLOW FOR PRESTACK SEPARATION

In order to combine the features of the prestack diffraction separation, we propose the following strategy to obtain diffraction-only data:

1. determine the CRS wavefield attributes,
2. search for the ZO time and the according CRS attributes that correspond to the offset under consideration,

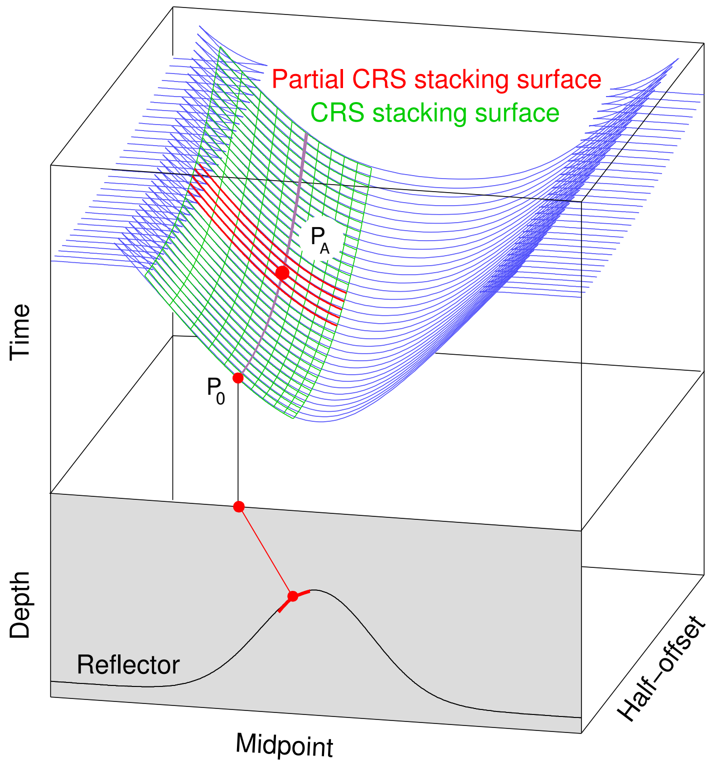

Figure 2: Sketch of a 2D model and the resulting data (modified after Müller, 1999): the blue lines represent the multicoverage data in the midpoint and half-offset domain. The purple line is the CRP stacking trajectory associated with the point P_0 and the red surface is the corresponding CRS stacking surface. In both cases, the stack result is assigned to the point P_0 with coordinates $(x_0, t_0, h = 0)$. For the prestack data enhancement with a partial CRS stack for a point P_A with coordinates $(x_0, t_A, h_A \neq 0)$, the traces are stacked along the red surface and assigned to the point P_A.

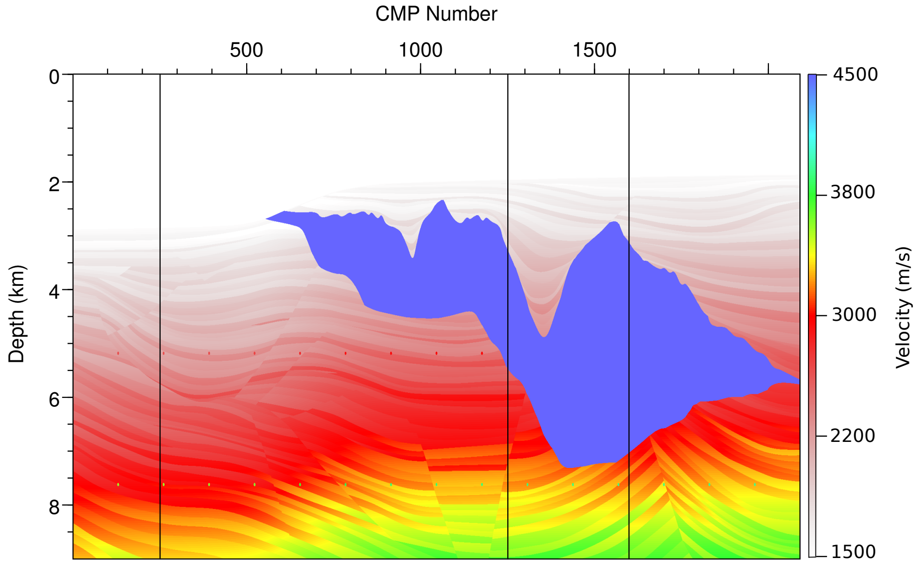

Figure 3: Velocity model for the Sigsbee 2A example. Vertical lines indicate CMP positions selected for detailed investigation (see Figure 5).

3. evaluate the separation criterion with a suitable choice of W_F,
4. perform the partial CDS stack.

In the following section, we apply this workflow to the complex synthetic Sigsbee 2A example as well as to field data from the Mediterranean.

EXAMPLES

In this section, we demonstrate the potential and advantages of the CRS-based prestack diffraction separation by applying it to the Sigsbee 2A synthetic data set and field data.

Sigsbee 2A synthetic data

In order to investigate the performance of our new workflow, we have chosen the Sigsbee 2A data set. Sigsbee 2A is a constant density acoustic synthetic data set developed by the SMAART JV consortium. It models the geologic setting found in the Sigsbee escarpment in the deep water Gulf of Mexico. The irregular boundaries of the salt body as well as faults in the model shown in Figure 3 cause strong diffractions. The data were modelled for a CMP interval of 11.43 m with a maximum fold of 87 and offsets up to 7932 m.

We have carried out the processing workflow that was introduced above with a threshold value of 0.9. Figure 4 shows the resulting CRS-stacked sections before (Figure 4a) and after (Figure 4b) the prestack diffraction separation. The diffracted events are considerably well separated. However, some residual reflection energy still is present.

For a more detailed investigation we have chosen three CMP's that illuminate different structural features of the data. Their positions are indicated in Figures 3 and 4a.

Figure 5a presents the results for CMP gather 250 in the left part of the model before and after diffraction separation. The diffractions in this region do not stem from the salt topography. They have low amplitudes and are masked by the stronger reflections. In the respective diffraction-only gather, these weak diffractions have been successfully separated from the reflections.

In Figure 5b, we show CMP gather 1250, which is located close to the rugged top of the salt and above a steep flank of the salt dome. Again, the separation of events has overall performed well. Some artifacts are still present, e.g., at 1000 m offset and 6 s TWT, where conflicting dips can be recognised in

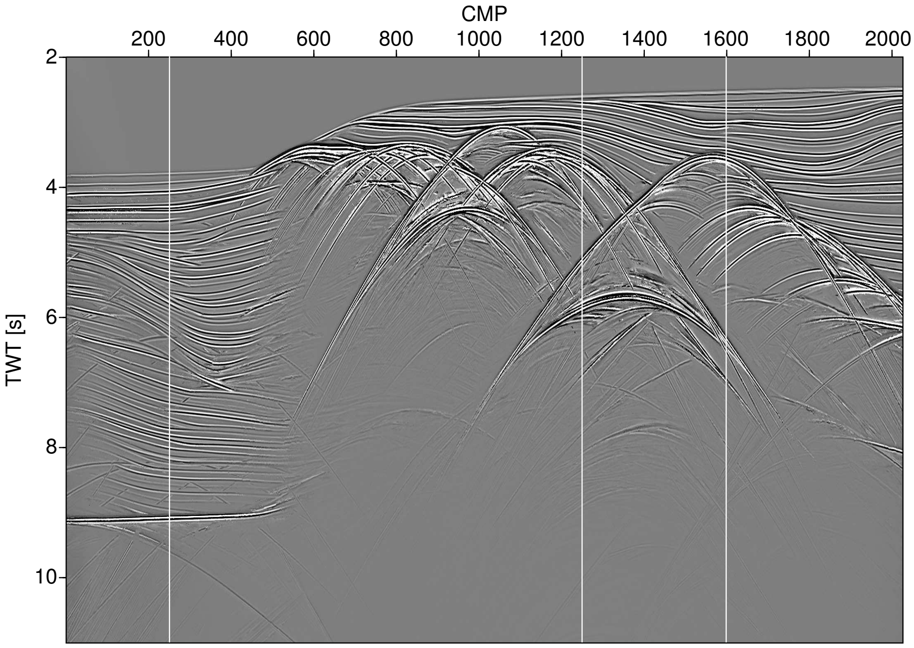

(a)

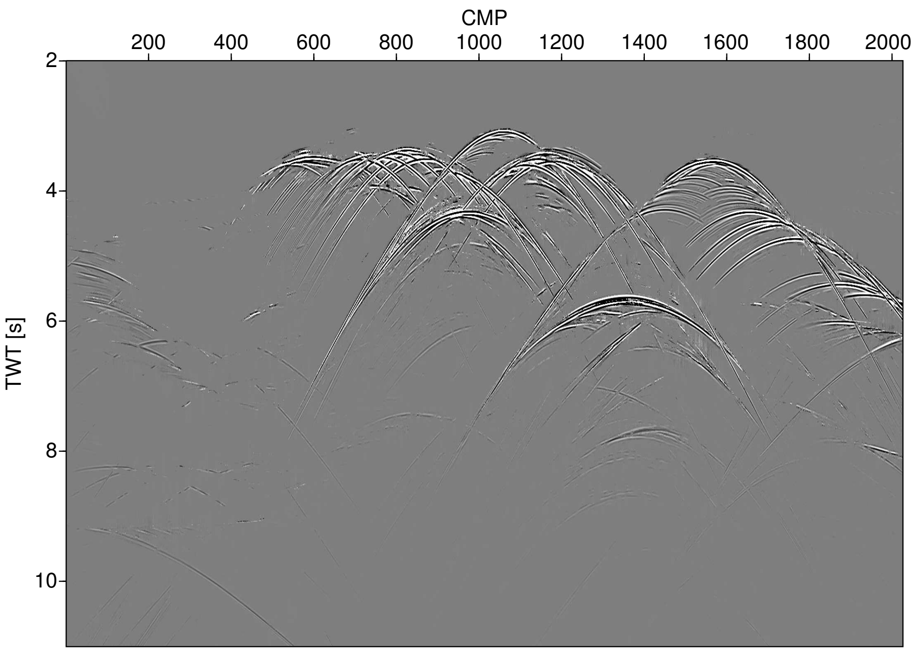

(b)

Figure 4: Sigsbee 2A example: ZO CRS-stacked section (a) before and (b) after prestack diffraction separation with a threshold value of 0.9. The vertical lines in (a) indicate CMP positions selected for detailed investigation (see Figure 5).

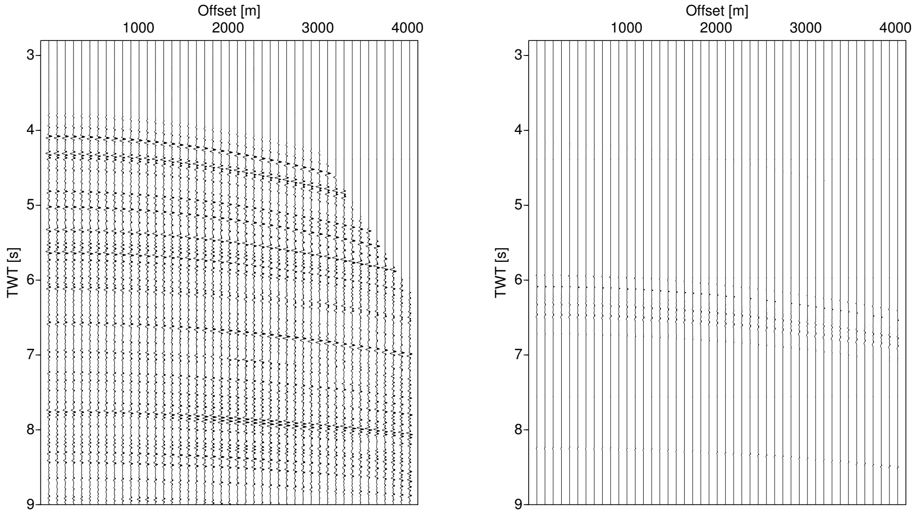

(a) CMP 250

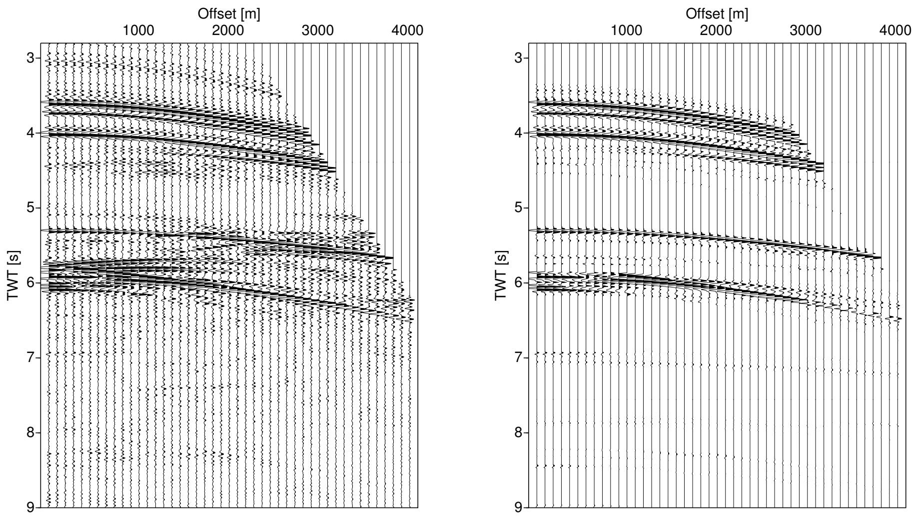

(b) CMP 1250

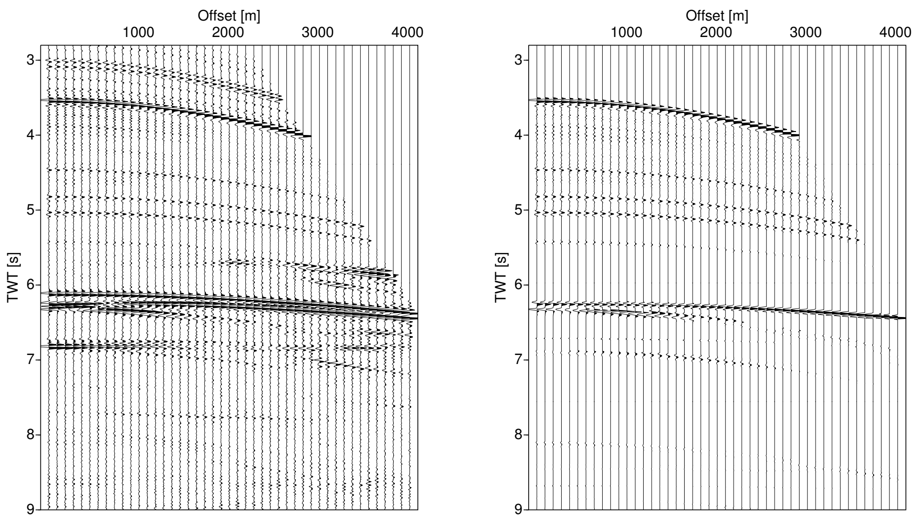

(c) CMP 1600

Figure 5: Sigsbee 2A example: CMP gathers (left) for CMP 250 (a), 1250 (b), and 1600 (c), respectively, and the corresponding diffraction-only gathers (right). The threshold for the separation was 0.9.

the section prior to separation. In order to successfully apply the new workflow to such regions, conflicting dip processing is required that was not considered in our current implementation.

Figure 5c displays CMP gather 1600 that contains reflections and diffractions of varying strength. Again, the reflections have been successfully eliminated in the diffraction-only gather.

Finally, an important application of the prestack diffraction separation is time migration velocity analysis. We have therefore taken a closer look at the velocity spectra resulting from CRS stacking before and after diffraction separation for CMP's 250 and 1250. They are shown in Figure 6 and demonstrate that we can achieve higher coherence values as well as better focusing by considering diffraction-only data. As pointed out above, these velocities can immediately be applied as time migration velocities since they no longer depend on the reflector dip.

Now that we have verified the method on synthetic data under controlled conditions, we apply it to field data in the following section.

Marine field data

In order to study the new workflow on field data, we chose a 2D marine data set from the central Levantine Basin located in the Eastern Mediterranean Sea. Figure 7 shows the geologic setting. The Levantine basin has a complex seismic stratigraphy of the basin succession. The deformation pattern of the intraevaporitic sequence include folds and thrust faulting, which gives evidence for extensive salt tectonic and shortening during the depositional phase. Postdepositional gravity gliding caused salt rollers in the extensional marginal domain, compressional folds, and faults within the Levantine Basin. More details can be found in Netzeband et al. (2006).

We have processed a subset of the data comprising 2000 CMP's, which represent roughly 15 km of the profile. The CMP interval was 12.5 m with offsets between 135 and 7325 m. In the stacked sections in Figure 8 we recognise a chain of diffractions mostly in the left part of the profile, from 2 to 3 s TWT. These are caused by salt rollers. Please note that because of the complex geological feature of the area, out-of-plane diffractions are also present mostly on the right part.

Again, we have chosen three CMP's for a more detailed investigation. Their positions are indicated in Figure 8a.

Figure 9a shows the results for CMP gather 2500 before and after diffraction separation. The strong diffractions, mostly around 2.3 s TWT, are caused by the rugged top of the salt. A number of weaker diffractions is also present. In Figure 9b, we display the results for CMP 2900. Strong diffraction events can be recognised between 2.5 and 3 s TWT after the separation. The third CMP gather at position 3800 is presented in Figure 9c. Again, several diffraction events are visible. The difference in move-out suggests that some of these diffractions correspond to out-of-plane events.

Not only do these results demonstrate that the prestack diffraction separation performs well. We also recognise that in all diffraction-only gathers in Figure 9 as well as in the stacked section in Figure 8b the signal-to-noise ratio is increased after the separation, which is due to the prestack data enhancement property of our workflow.

As a final investigation of the field data, we have generated velocity spectra prior to and after diffraction separation. These are shown in Figure 10 for CMP's 2500 and 2900. We recognise maxima that are well-focused prior to the separation for TWT up to 2.5 s. The diffraction-only stacks lead to spectra that contain distinct maxima at higher TWT, which cannot be identified in the spectra prior to the separation. This shows again that diffraction-only data can play an important role for the determination of time migration velocities.

CONCLUSIONS

In this paper, we have introduced a new workflow for the generation of diffraction-only prestack data. The workflow combines the method of diffraction separation with the partial CRS stack technique. After verifying the workflow under controlled conditions to the synthetic Sigsbee 2A data, we applied it to a 2D marine field data set. The separation of diffraction events performed well for both data sets, leading to diffraction-only prestack sections with an enhanced signal-to-noise ratio.

Furthermore, stacking velocity analysis of the diffraction-only data leads to well-focused spectra that

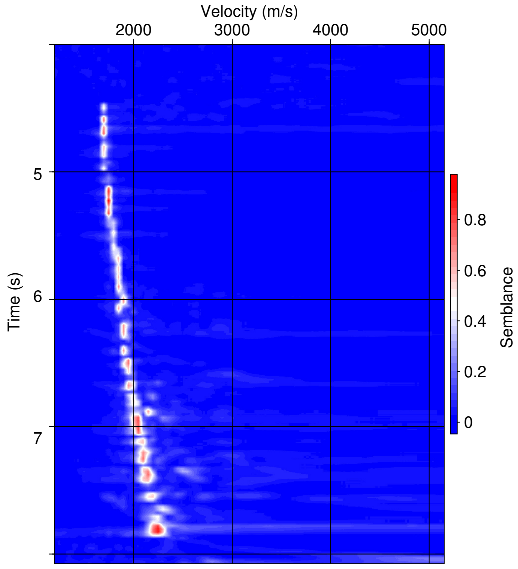

(a) CMP 250

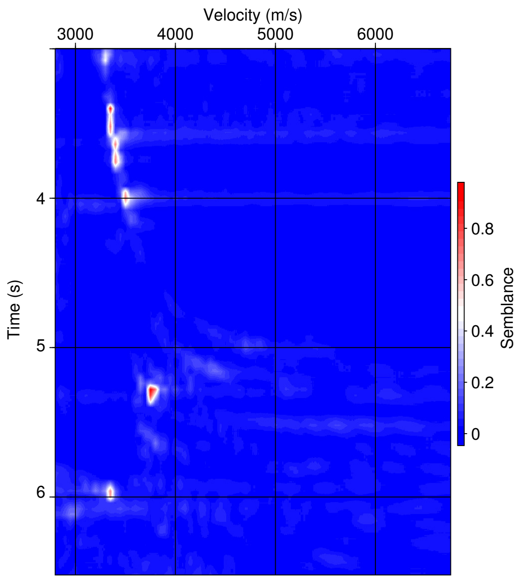

(b) CMP 1250

Figure 6: Sigsbee 2A example: velocity spectra for CMP 250 (a) and 1250 (b) before (left) and after (right) prestack diffraction separation.

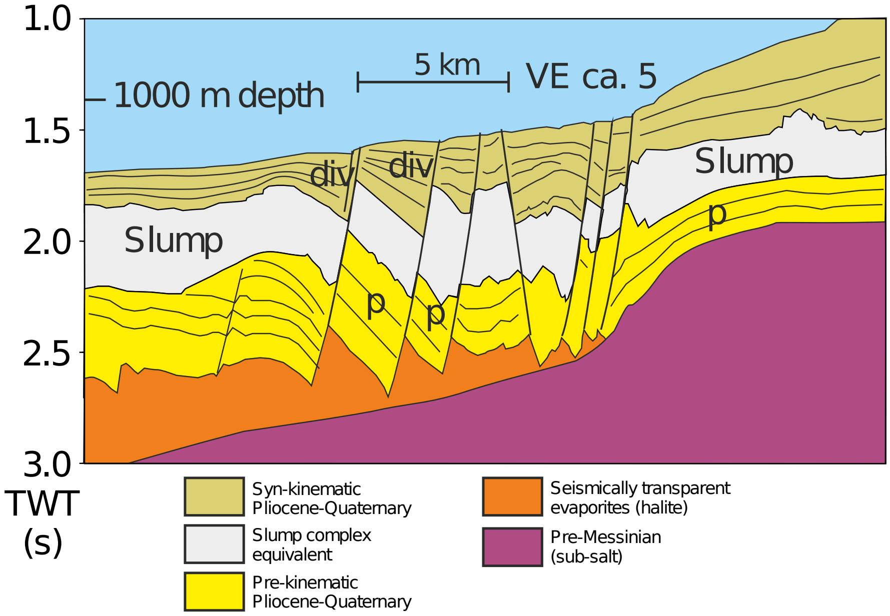

Figure 7: Geologic setting for the marine field data example (Netzeband et al., 2006).

allow the determination of velocities that, in contrast to stacking velocities from reflection data, no longer depend on reflector dips. This means that stacking velocities obtained from diffraction-only data can be directly applied for time migration without need for further migration velocity analysis.

ACKNOWLEDGEMENTS

We thank the members of the Applied Seismics Group Hamburg for continuous discussions. The Sigsbee A data set was provided by the SMAART Joint Venture and the field data by TGS-NOPEC. This work was partially supported by the sponsors of the WIT consortium.

REFERENCES

Baykulov, M. and Gajewski, D. (2009). Prestack data enhancement with partial common reflection surface (CRS) stack. *Geophysics*, 74:V49–V58.

Dell, S. (2012). *Seismic processing and imaging with diffractions*. PhD thesis, University of Hamburg.

Dell, S. and Gajewski, D. (2011). Common-reflection-surface-based workflow for diffraction imaging. *Geophysics*, 76:S187–S195.

Dell, S., Vanelle, C., and Gajewski, D. (2012). Prestack time migration by common-migrated-reflector-element stacking. *Geophysics*, 77:S73–S82.

Fomel, S., Landa, E., and Taner, M. T. (2006). Poststack velocity analysis by separation and imaging of seismic diffractions. *Geophysics*, 72:U89–U94.

Guntern, C. (2013). Bearbeitung reflexionsseismischer Daten unter besonderer Berücksichtigung von Diffraktionen. Bachelor's thesis, University of Hamburg.

Mann, J. (2002). *Extensions and Applications of the Common-Reflection-Surface Stack Method*. PhD thesis, University of Karlsruhe.

Müller, T. (1999). *The Common Reflection Surface stack method – Seismic imaging without explicit knowledge of the velocity model*. PhD thesis, University of Karlsruhe.

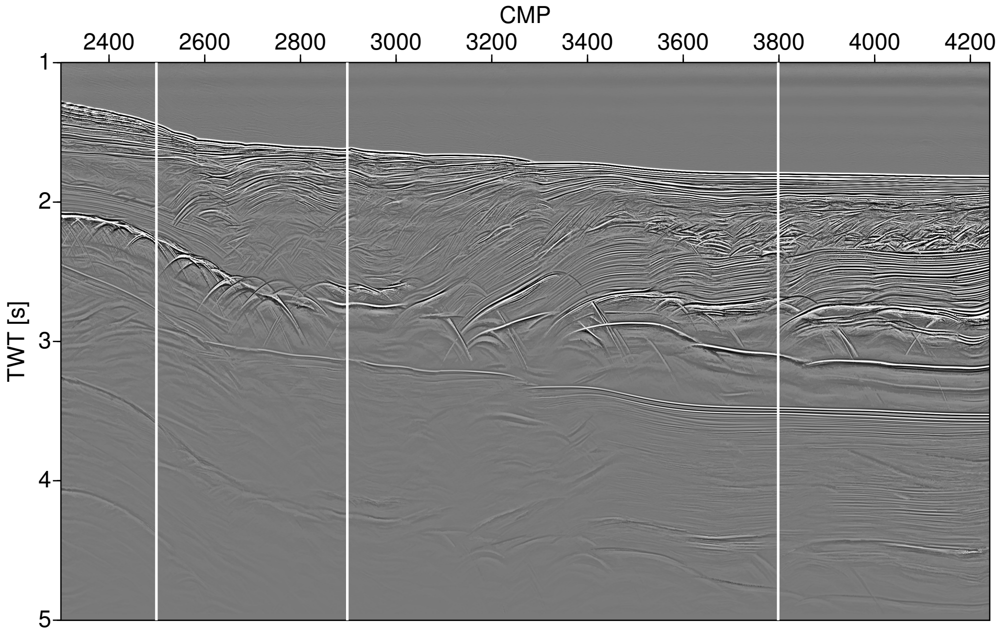

(a)

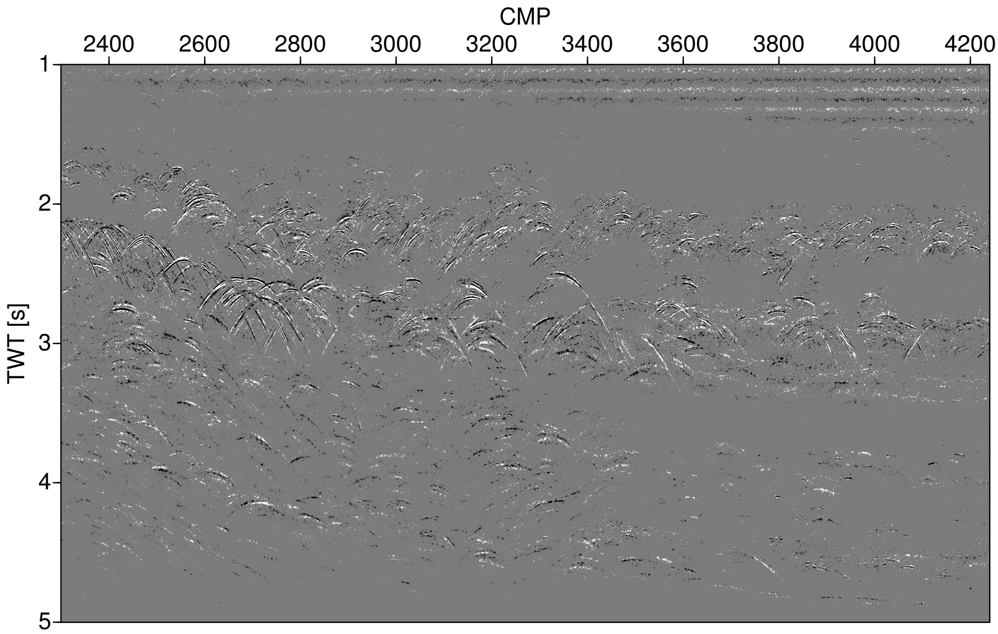

(b)

Figure 8: Field data example: ZO CRS-stacked section (a) before and (b) after prestack diffraction separation with a threshold value of 0.85. The vertical lines in (a) indicate CMP positions selected for detailed investigation (see Figure 9).

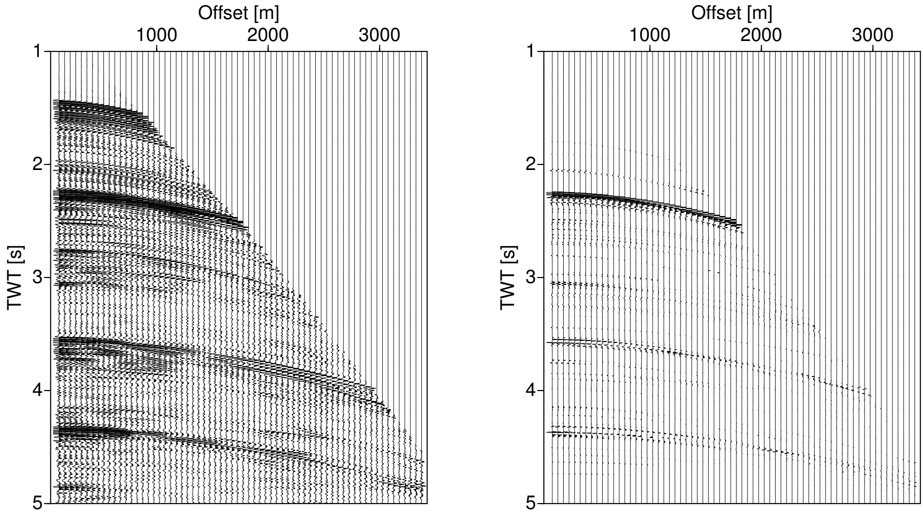

(a) CMP 2500

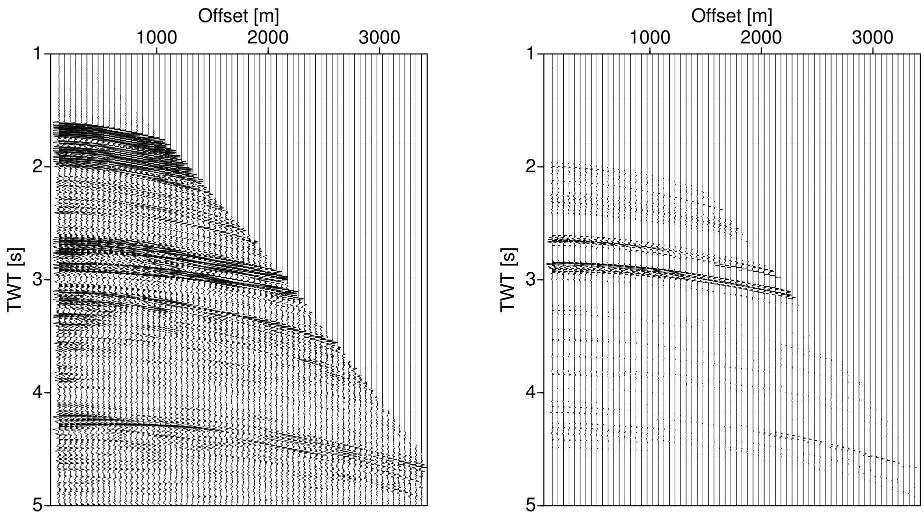

(b) CMP 2900

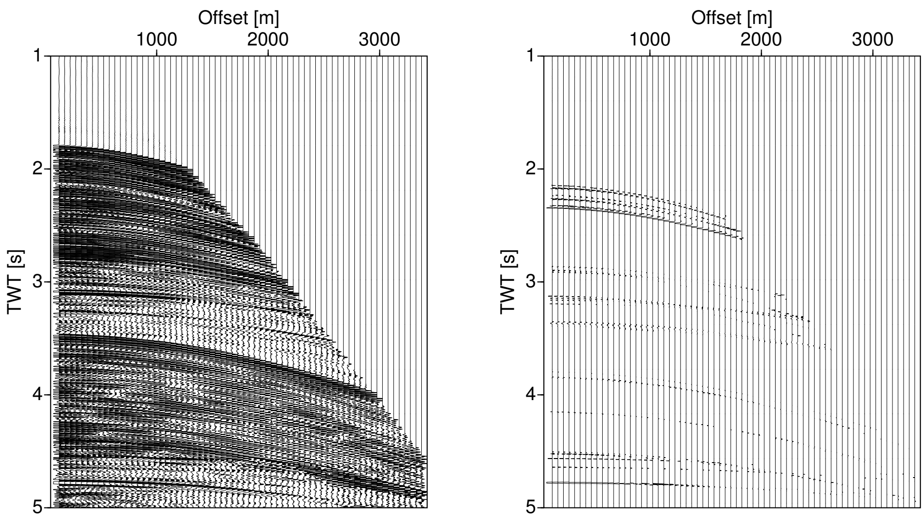

(c) CMP 3800

Figure 9: Field data example: CMP gathers (left) for CMP 2500 (a), 2900 (b), and 3800 (c), respectively, and the corresponding diffraction-only gathers (right). The threshold for the separation was 0.85.

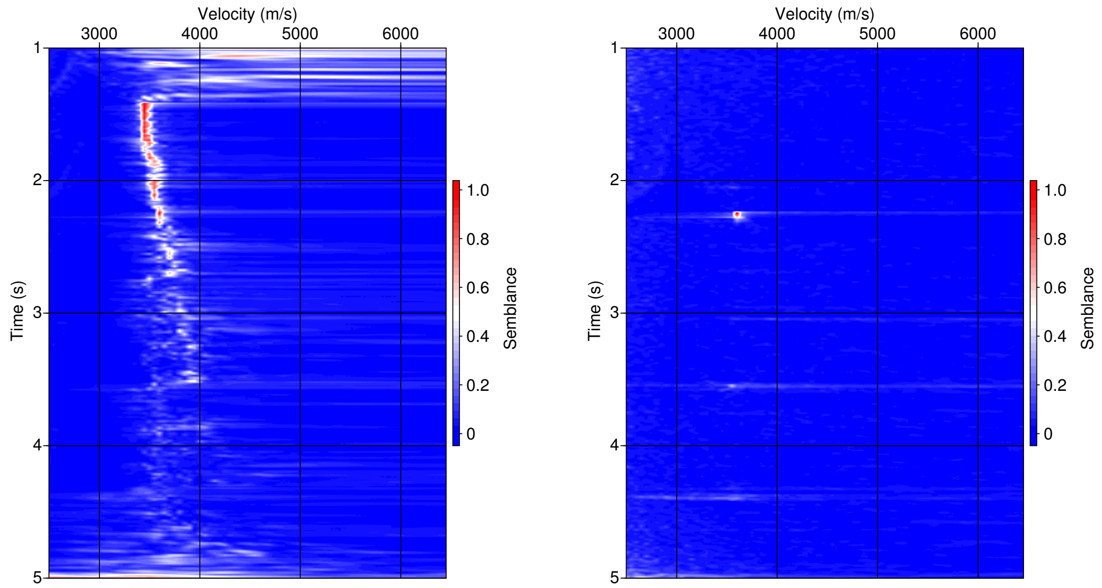

(a) CMP 2500

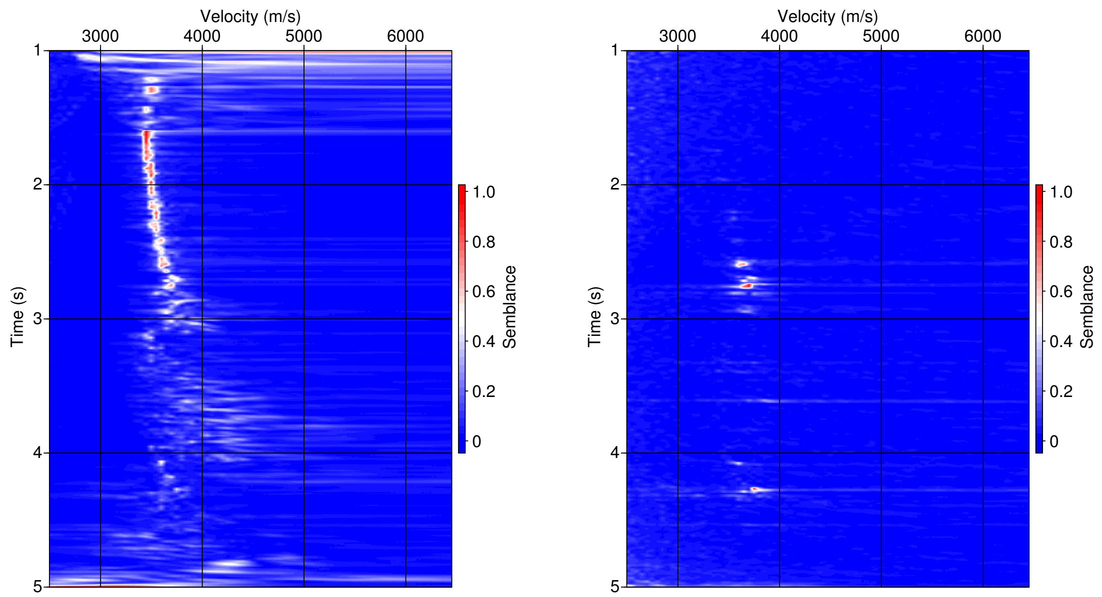

(b) CMP 2900

Figure 10: Field data example: velocity spectrum for CMP 2500 (a) and 2900 (b), respectively, before (left) and after (right) prestack diffraction separation. The threshold for the separation was 0.85.

Netzeband, G., Gohl, K., Hübscher, C., Dehghani, A., Gajewski, D., and Liersch, P. (2006). The Levantine basin – crustal structure and origin of the Messinian evaporites in the Levantine basin. *Tectonophysics*, 418:167–188.

Schleicher, J., Tygel, M., and Hubral, P. (1993). Parabolic and hyperbolic paraxial two-point traveltimes in 3D media. *Geophysical Prospecting*, 41:495–514.

Soleimani, M., Mann, J., Adibi Sede, E., and Piruz, I. (2010). Improving the seismic image quality in semicomplex structures in north east iran by the cds stack method. *72nd Annual International Meeting, EAGE, Expanded Abstracts*, page A39.

Voß, M. (2013). Bearbeitung reflexionsseismischer Daten unter besonderer Berücksichtigung von Diffraktionen. Bachelor's thesis, University of Hamburg.